\



Pressure- and temperature-dependent luminescence from Tm^{3+} ions doped in $GdYTaO_4$

Peng-Yu Zhou(周鹏宇), Xiu-Ming Dou(窦秀明), Bao-Quan Sun(孙宝权), Ren-Qin Dou(窦仁琴), Qing-Li Zhang(张庆礼), Bao Liu(刘鲍), Pu-Geng Hou(侯朴赓), Kai-Lin Chi(迟凯鄰), and Kun Ding(丁琨)

Citation: Chin. Phys. B, 2022, 31 (**1**): 017101. DOI: 10.1088/1674-1056/ac0526
Journal homepage: http://cpb.iphy.ac.cn; http://iopscience.iop.org/cpb

What follows is a list of articles you may be interested in

Mechanism of free electron concentration saturation phenomenon in Te-GaSb single crystal

Ding Yu(余丁), Guiying Shen(沈桂英), Hui Xie(谢辉), Jingming Liu(刘京明), Jing Sun(孙静), Youwen Zhao(赵有文)
Chin. Phys. B, 2019, 28 (**5**): 057102. DOI: 10.1088/1674-1056/28/5/057102

Optical characterization of defects in narrow-gap HgCdTe for infrared detector applications

Fang-Yu Yue(越方禹), Su-Yu Ma(马骕驭), Jin Hong(洪进), Ping-Xiong Yang(杨平雄), Cheng-Bin Jing(敬承斌), Ye Chen(陈晔), Jun-Hao Chu(褚君浩)
Chin. Phys. B, 2019, 28 (**1**): 017104. DOI: 10.1088/1674-1056/28/1/017104

Photoluminescence in fluorescent 4H-SiC single crystal adjusted by B, Al, and N ternary dopants

Shi-Yi Zhuo(卓世异), Xue-Chao Liu(刘学超), Wei Huang(黄维), Hai-Kuan Kong(孔海宽), Jun Xin(忻隽), Er-Wei Shi(施尔畏)
Chin. Phys. B, 2019, 28 (**1**): 017101. DOI: 10.1088/1674-1056/28/1/017101

Visualizing light-to-electricity conversion process in InGaN/GaN multi-quantum wells with a p-n junction

Yangfeng Li(李阳锋), Yang Jiang(江洋), Junhui Die(迭俊珲), Caiwei Wang(王彩玮), Shen Yan(严珅), Haiyan Wu(吴海燕), Ziguang Ma(马紫光), Lu Wang(王禄), Haiqiang Jia(贾海强), Wenxin Wang(王文新), Hong Chen(陈弘)
Chin. Phys. B, 2018, 27 (**9**): 097104. DOI: 10.1088/1674-1056/27/9/097104

Characterization of deep acceptor level in as-grown ZnO thin film by molecular beam epitaxy

M. Asghar, K. Mahmood, M. A. Hasan, I. T. Ferguson, R. Tsu, M. Willder
Chin. Phys. B, 2014, 23 (**9**): 097101. DOI: 10.1088/1674-1056/23/9/097101

Pressure- and temperature-dependent luminescence from Tm^{3+} ions doped in $GdYTaO_4$

Peng-Yu Zhou(周鹏宇)[1,†], Xiu-Ming Dou(窦秀明)[2], Bao-Quan Sun(孙宝权)[2], Ren-Qin Dou(窦仁琴)[3], Qing-Li Zhang(张庆礼)[3], Bao Liu(刘鲍)[1], Pu-Geng Hou(侯朴赓)[1], Kai-Lin Chi(迟凯粼)[1], and Kun Ding(丁琨)[2]

[1] *School of Science, Northeast Electric Power University, Jilin* 132012, *China*
[2] *State Key Laboratory of Superlattices and Microstructures, Institute of Semiconductors, Chinese Academy of Sciences, Beijing* 100083, *China*
[3] *Key Laboratory of Photonic Devices and Materials, Anhui Institute of Optics and Fine Mechanics, Chinese Academy of Sciences, Hefei* 230031, *China*

(Received 20 March 2021; revised manuscript received 7 May 2021; accepted manuscript online 26 May 2021)

Luminescent properties of Tm^{3+}-doped $GdYTaO_4$ are studied for exploring their potential applications in temperature and pressure sensing. Two main emission peaks from $^3H_4 \rightarrow {}^3H_6$ transition of Tm^{3+} are investigated. Intensity ratio between the two peaks evolves exponentially with temperature and has a highest sensitivity of 0.014 K^{-1} at 32 K. The energy difference between the two peaks increases linearly with pressure increasing at a rate of 0.38 meV/GPa. Intensity ratio between the two peaks and their emission lifetimes are also analyzed for discussing the pressure-induced variation of the sample structure. Moreover, Raman spectra recorded under high pressures indicate an isostructural phase transition of $GdYTaO_4$ occurring at 4.46 GPa.

Keywords: rare-earth tantalate, photoluminescence, high pressure, Raman

PACS: 71.20.Eh, 78.55.–m, 62.50.–p, 78.30.–j **DOI:** 10.1088/1674-1056/ac0526

1. Introduction

In recent years, researches about the spectra of Tm^{3+}-doped materials have been continually intensified for their potential applications. Owing to its rich energy levels, Tm^{3+} ion exhibits outstanding up-conversion for near-infrared (NIR) excitations[1–3] and down-conversion for ultraviolet (UV) excitations.[4–6] With the up-conversion mechanism and the down-conversion mechanism, Tm^{3+}-doped materials can generate UV emissions by $^1D_2 \rightarrow {}^3H_6$ transition, blue emissions by $^1D_2 \rightarrow {}^3F_4$ transition, blue–green emissions by $^1G_4 \rightarrow {}^3H_6$ transition, red emissions by $^1G_4 \rightarrow {}^3H_4$ and $^3F_{2,3} \rightarrow {}^3H_6$ transitions, NIR emissions by $^3H_4 \rightarrow {}^3H_6$ and $^3F_4 \rightarrow {}^3H_6$ transitions, making them valuable for applications in optical display,[1,4,6] optical sensing,[1,6] lighting,[1,4,6] biological labeling,[1–3,7] quantum efficiency enhancing for solar cells,[2,4,5] fiber optics, and medical surgery.[8]

Rare-earth tantalates with $LnTaO_4$ (Ln = Y, Gd, La, Sc, Lu) stoichiometry are promising host materials for rare-earth activator ions,[9–12] which have high density and hardness values,[9,13,14] high x-ray and UV absorptions,[11–13] high chemical and physical stabilities.[9–14] Moreover, owing to the low symmetry and strong crystal field of this kind of host, activator ions doped can have a high photoluminescence (PL) efficiency.[9–12] Considering these advantages, $LnTaO_4$ could be promising hosts for Tm^{3+} ions. The structural stability and thermodynamic properties of $LnTaO_4$ were partially investigated.[9,10,13,14] Extensive studies still need to be performed on this kind of material, to understand the mechanical and structural properties and the luminescent properties of activator ions doped.

In this work, luminescent properties of Tm^{3+}-doped $GdYTaO_4$ are studied with emphasis on its dependence of temperature and pressure to explore its potential applications. Moreover, to further understand the pressure-dependent behavior of PL intensity of the doped Tm^{3+} ions and the structural stability of the host, high-pressure Raman spectra of $GdYTaO_4$ are measured and analyzed.

2. Experiment

The sample for PL measurements was cleaved from a Tm^{3+}:$GdYTaO_4$ crystal[10] grown by the Czochralski method. In the corresponding precursor, molar ratio of metal ions Tm^{3+}:Y^{3+}:Gd^{3+}:Ta^{5+} was 1:10:39:50.[10] A $GdYTaO_4$ sample and two reference samples $LnTaO_4$ (Ln = Gd, Y) were prepared by the solid-phase reaction method for Raman measurements. The precursor of $GdYTaO_4$ was a mixture of Y_2O_3, Gd_2O_3, and Ta_2O_5, with a molar ratio of 1:4:5. The precursor of $LnTaO_4$ was a mixture of Ln_2O_3 and Ta_2O_5, with a molar ratio of 1:1. All these precursors were thoroughly ground and sintered at 1550 °C for 12 h, then naturally cooled down to room temperature. To facilitate the subsequent tests, all these samples were finely powdered by ball milling (Pulverisette 6,

†Corresponding author. E-mail: 20162715@neepu.edu.cn

© 2022 Chinese Physical Society and IOP Publishing Ltd

FRITSCH). Room temperature and low temperature structures of Tm^{3+}:$GdYTaO_4$ were characterized using an x-ray diffractometer (TTR3, Rigaku), while room temperature structures of $GdYTaO_4$, $GdTaO_4$, and $YTaO_4$ were characterized using another x-ray diffractometer (DX-2700B, Haoyuan Instrument).

High pressure was generated using a diamond anvil cell (DAC). A 250-μm hole mechanically drilled in a stainless steel gasket was used as sample chamber. A little of a sample powder was loaded into the chamber by a needle. A 4:1 methanol-ethanol mixture was used as the pressure-transmitting medium, which was hydrostatic up to 10 GPa.[15] The pressure value was determined using the ruby luminescence technique.[16]

For PL measurements, a 454-nm diode laser was used as excitation source, and the incident power was 0.3 mW. For Raman measurements, a 632.8-nm He–Ne laser was used as excitation source, the incident power is 3 mW. All spectra were measured using a spectrometer consisting of a monochromator (HRS-500MS-NI, Princeton Instruments) with a focal length of 0.5 m and a Peltier-cooled silicon charge-coupled device (PIX-400BRX, Princeton Instruments). The corresponding spectral resolution was better than 2 cm^{-1}. Moreover, a cryostat (Montana Instruments) was used for the varying temperature PL measurements.

For time-resolved PL measurements, an acousto–optical modulator (AOM) triggered by a signal generator with a frequency of 500 Hz was used to periodically switch the path of the exciting laser to realize a pulsed excitation. In each cycle, the sample was excited first by the laser as the AOM was on with a duration of 10 μs. Then the laser was switched to somewhere as the AOM was off with a duration of 990 μs. The sample PL was selected using the monochromator and sent to a silicon avalanche photodiode (Si-APD). The Si-APD output was input into a multi-channel scaler triggered by the signal generator and synchronized with the pulsed excitation. The measuring time range was 2 ms, the width of each time bin was 0.5 μs. Such a time resolution of the setup enabled us to study the PL dynamic of Tm^{3+}:$GdYTaO_4$.

3. Results and discussion

The x-ray diffraction (XRD) patterns of Tm^{3+}:$GdYTaO_4$ at 300 K and 77 K, shown in Fig. 1(a), are both consistent with the ICDD card file 24441, indicating that the sample studied has a monoclinic fergusonite structure belonging to $I2/a$ space group symmetry (or M-type phase for short) in a broad temperature range. Structure diagrams of M-type Tm^{3+}:$GdYTaO_4$ are shown in Fig. 1(b). In this structure, each Ln (Ln = Gd, Y, Tm) atom is coordinated by eight O atoms, forming an LnO_8 dodecahedron, while each Ta atom is coordinated by four O atoms, forming a TaO_4 tetrahedron. The LnO_8 dodecahedra are arranged in edge-sharing zig-zag chains along both the a and c axes. The zig-zag shift is directed along the b axis. The TaO_4 tetrahedra are located in the space defined by the zig-zag chains and share corners with four adjacent LnO_8 dodecahedra. The lattice parameters of Tm^{3+}:$GdYTaO_4$ were obtained using the Rietveld refinement method:[9] $a = 5.39$ Å, $b = 11.03$ Å, $c = 5.08$ Å, and $\beta = 95.61°$. More information about the structure can be found in Refs. [9,10].

Under the 454-nm excitation, the intense emissions from $^3H_4 \rightarrow {}^3H_6$ transition of Tm^{3+} [4,5,7] in $GdYTaO_4$ are observed (see Fig. 1(c)). These emissions just lie in the first biological window 750 nm–950 nm, which allows for deep light penetration and producing a high biological labeling contrast.[3] Moreover, as the figure shows, a diode laser with a longer wavelength (such as 640 nm) can also be used as excitation source to obtain emission of $^3H_4 \rightarrow {}^3H_6$ transition, indicating that the potential applications of Tm^{3+}:$GdYTaO_4$ is flexible.

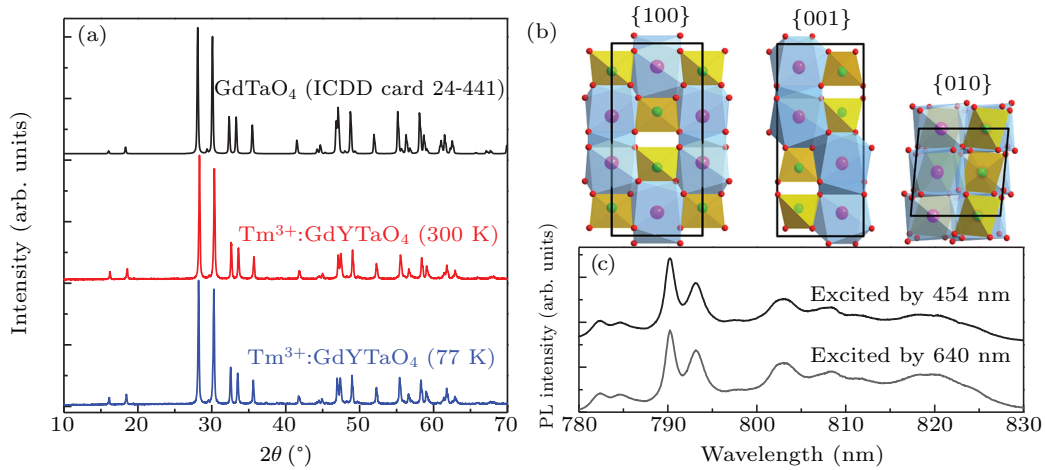


Fig. 1. (a) XRD patterns of Tm^{3+}:$GdYTaO_4$ measured at 300 K and 77 K, under zero pressure. The standard XRD pattern of M-type $GdTaO_4$ at ambient condition is also depicted. (b) Structural projections on {100}, {001}, and {010} planes for Tm^{3+}:$GdYTaO_4$. Purple spheres represent Ln (Ln = Gd, Y, Tm) atoms; green spheres represent Ta atoms; small red spheres denote O atoms. (c) PL spectra of Tm^{3+}:$GdYTaO_4$ under ambient condition, measured using 454-nm and 640-nm lasers as excitation source.

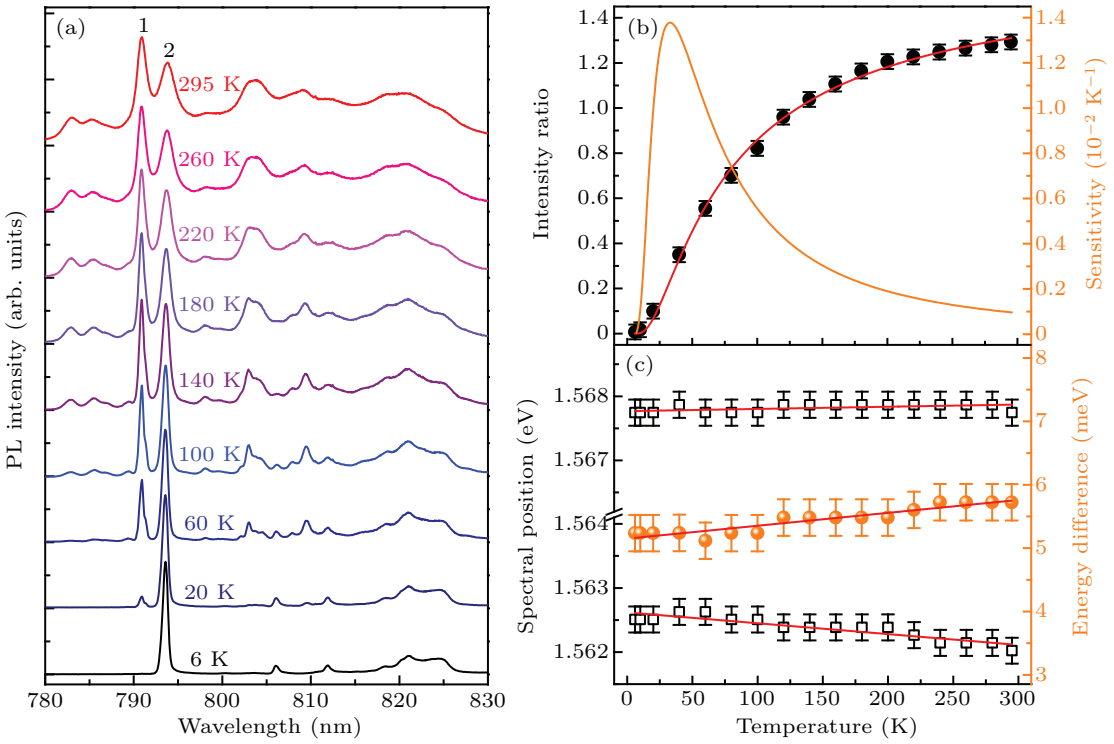


Fig. 2. (a) Normalized PL spectra of $^3H_4 \rightarrow {}^3H_6$ transition of Tm^{3+}:$GdYTaO_4$ at zero pressure and various temperatures. (b) Intensity ratio I_1/I_2 between peaks 1 and 2 (solid black circles) and temperature sensitivity of I_1/I_2 (orange line) each as a function of temperature. (c) Spectral positions of peaks 1 and 2 (open black squares) and their energy difference (solid orange balls) each as a function of temperature. Red lines in panels (b) and (c) represent fitting curves. Error bars in panels (b) and (c) denote the experimental uncertainties in the determination of the corresponding data.

Temperature-dependent PL of Tm^{3+}:$GdYTaO_4$ is studied, some representative spectra recorded are shown in Fig. 2(a). As temperature decreases, the intensity of the peak at $\sim$ 790 nm (peak 1) decreases, while intensity of the peak at $\sim$ 793 nm (peak 2) increases. The relative change of intensities of the two peaks indicates the population change of the higher and the lower Stark levels of $^3H_4$. The intensity ratios I_1/I_2 between peaks 1 and 2 at different temperatures are calculated (see Fig. 2(b)), and then fitted using a Boltzmann-type population distribution function[17]

$$I_1/I_2 = N\exp\left(-\frac{\Delta E}{kT}\right), \tag{1}$$

where I_1 and I_2 are the maximum intensities of peaks 1 and 2, respectively; N is a constant; ΔE is the energy gap of the thermally coupled levels; k is the Boltzmann constant; T is the absolute temperature. The fitting result is $I_1/I_2 = (1.63 \pm 0.02)\exp[-(64 \pm 2)/T]$. The fitted ΔE value is 5.5 ± 0.2 meV, which is consistent with the value 5.8 meV measured under ambient condition, and similar to that of Tm^{3+}:$Y_3Al_5O_{12}$.[18] Based on the fitting result, the temperature sensitivity of I_1/I_2 is calculated from the following equation:[17]

$$\frac{\mathrm{d}(I_1/I_2)}{\mathrm{d}T} = N\frac{\Delta E}{kT^2}\exp\left(-\frac{\Delta E}{kT}\right). \tag{2}$$

As figure 2(b) shows, the maximum sensitivity of I_1/I_2 is 0.014 K^{-1} at 32 K. Moreover, thermal shifts of peaks 1 and 2 are also analyzed. As figure 2(c) shows, peak 1 shifts little, while peak 2 shifts toward the lower energy side slowly with temperature increasing. This leads the energy difference between the two peaks to increase linearly with temperature increasing at a rate of 2.0 ± 0.2 μeV/K.

PL spectra of Tm^{3+}:$GdYTaO_4$ under high pressures up to $\sim$ 8 GPa are measured. As figure 3(a) shows, these emission peaks shift linearly with pressure increasing. Compared with the emission peaks in the shorter wavelength range, the emission peaks in the longer wavelength range exhibit more obvious red-shift, resulting in a broader emission band at a higher pressure. This indicates that the overall splitting of the corresponding Stark levels increases with pressure rising, which is due to pressure-induced decreases of Tm–O bond lengths enhancing the crystal-field strength around Tm^{3+} ions.[19] Pressure coefficients of peaks 1 and 2 are obtained based on linear fitting for the spectral position data (see Fig. 3(b)), which are 0.18 meV/GPa and −0.21 meV/GPa. The absolute value of pressure coefficient of peak 2 is larger than that of Tm^{3+}:$Y_3Al_5O_{12}$[19] and less than that of Tm^{3+}:$LiNbO_3$.[7] However, in this spectral range, a relatively large pressure-induced blue-shift behavior, just like peak 1, is not observed for these two materials. The opposite shifts of peaks 1 and 2 make the energy difference between peaks 1 and 2 increase linearly with pressure increasing (see Fig. 3(b)), which can be described as

$$\Delta E_\mathrm{p} = (5.83 \pm 0.06) + (0.38 \pm 0.01) \times P, \tag{3}$$

where ΔE_p is energy difference between peaks 1 and 2 in unit meV, P is pressure in unit GPa. It should be noted that ΔE_p can be a good parameter for pressure sensing. Compared with the traditional method of optical pressure sensing based on spectral shift of a single emission peak of ruby,[16] the method based on ΔE_p has a self-referencing feature and will be more convenient for use. Once a spectrum of Tm^{3+}:$GdYTaO_4$ is obtained, the corresponding pressure value can be ascertained without needing any reference parameter value at ambient pressure. Moreover, the temperature sensitivity 2.0 μeV/K (∼ 0.001 nm/K) of ΔE_p (see Fig. 2(c)) is much less than that of ruby emission peaks (0.0068 nm/K[20]), indicating that the method proposed has a higher anti-interference capability for temperature fluctuation. The pressure sensitivity of ΔE_p is 0.38 meV/GPa, which is less than that of ruby emission peaks (0.92 meV/GPa[20]), but it is good enough to use the Tm^{3+}:$GdYTaO_4$ as an optical pressure sensor in the NIR range.

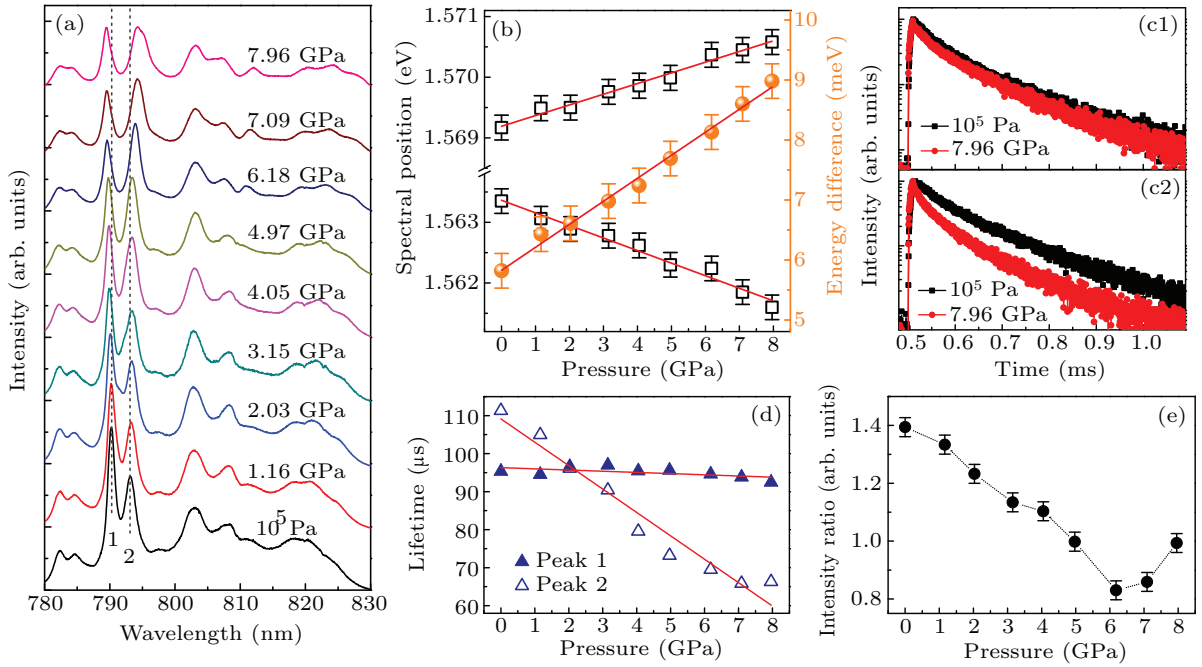


Fig. 3. (a) PL spectra of $^3H_4 \rightarrow {}^3H_6$ transition of Tm^{3+}:$GdYTaO_4$ at room temperature and various pressures. (b) Spectral positions of peaks 1 and 2 (open black squares) and their energy difference (solid orange balls) each as a function of temperature. (c1) PL decay curves of peak 1 at ambient pressure and 7.96 GPa. (c2) PL decay curves of peak 2 at ambient pressure and 7.96 GPa. (d) Effective emission lifetimes of peaks 1 and 2 each as a function of pressure. (e) I_1/I_2 as a function of pressure. Gray dashed lines in panel (a) indicate the positions of peaks 1 and 2 at ambient pressure. Red lines in panels (b) and (d) denote linear fitting curves. Longitudinal axes in panels (c1) and (c2) are in logarithmic scale. Error bars in panels (b) and (e) refer to the experimental uncertainties in the determination of the corresponding data.

To gain an insight into the PL dynamics of the Tm^{3+}:$GdYTaO_4$ under pressure, the time-resolved PL spectrum is also traced. The PL decay curves of peaks 1 and 2 measured at ambient pressure and 7.96 GPa are presented in Figs. 3(c1) and 3(c2), respectively. These decay curves are non-single-exponential, which is due to the cross relaxation (CR) among adjacent Tm^{3+} ions.[4,5] The effective emission lifetimes at different pressures are calculated from the following equation:[4,5]

$$\tau_{\text{eff}} = \frac{1}{I_0}\int_0^{\infty} I(t)\,\mathrm{d}t, \tag{4}$$

where $I(t)$ is the PL intensity as a function of time t, I_0 is the initial PL intensity. As figure 3(d) shows, the emission lifetimes of peaks 1 and 2 decrease with pressure increasing, the estimated pressure coefficients are −0.3 μs/GPa and −6.5 μs/GPa. The decreases of emission lifetime and PL intensity should be mainly due to the enhancement of CR process.[4,5,7,10] Specifically, the CR process is a process of energy transferring from a Tm^{3+} ion in the excited state $^3H_4$ to a nearby Tm^{3+} ion in the ground state $^3H_6$, resulting in the two ions both populating the intermediate state $^3F_4$.[7,10] The probability of CR can be elevated by pressure mainly through reducing the Tm^{3+}–Tm^{3+} distances and increasing the overlap integral between $^3H_4 \rightarrow {}^3F_4$ and $^3H_6 \rightarrow {}^3F_4$ transitions.[7] Therefore, a more active CR process at a higher pressure can lead the population of $^3H_4$ then the lifetime of $^3H_4$ and the emission intensity of $^3H_4 \rightarrow {}^3H_6$ to decrease. Moreover, the difference between the pressure coefficients of emission lifetimes of peaks 1 and 2 indicates that the corresponding Stark levels of $^3H_4$ have different sensitivities to the pressure-induced enhancement of the CR process.

The pressure evolution of I_1/I_2 is also investigated. As figure 3(e) shows, I_1/I_2 decreases in a pressure range up to 6 GPa, and increases with pressure increasing beyond 6 GPa. The discontinuity in the evolution of I_1/I_2 may indicate a phase transition for the host occurring at a pressure less than

6 GPa.

According to the non-monotonic evolution of I_1/I_2, Raman measurements are conducted to explore the structure variation of $GdYTaO_4$ under pressure. The phases of $GdYTaO_4$, $GdTaO_4$, and $YTaO_4$ samples under ambient condition are ascertained using XRD measurements. As figure 4(a) shows, the XRD patterns of $GdYTaO_4$ and $GdTaO_4$ are consistent with the ICDD card file 24-441, and the XRD pattern of $YTaO_4$ is consistent with the ICDD card file 24-1415, indicating that the three samples are all of M-type phase. Raman spectra of the three samples are shown in Fig. 4(b). According to theoretical studies,[21,22] M-type $GdTaO_4$ and $YTaO_4$ both have 18 Raman-active modes in the center of the Brillouin zone:

$$\Gamma = 8A_g + 10B_g, \tag{5}$$

where A_g and B_g modes represent parallel- and cross-polarized Raman scattering, respectively. By comparison, the Raman spectrum of $GdYTaO_4$ is more similar to that of $GdTaO_4$ than that of $YTaO_4$. However, the Raman modes of $GdYTaO_4$ in 100 cm^{-1}–200 cm^{-1} are weaker and broader, which should be due to the increasing of the disorders of the external vibrations of TaO_4 tetrahedra,[21–23] induced by the portion of Y^{3+} ions.

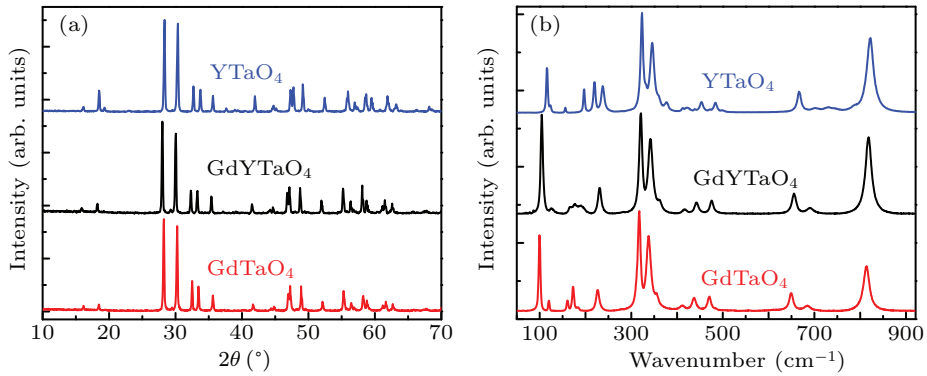


Fig. 4. (a) XRD patterns and (b) Raman spectra of $GdTaO_4$, $GdYTaO_4$, and $YTaO_4$ under ambient condition.

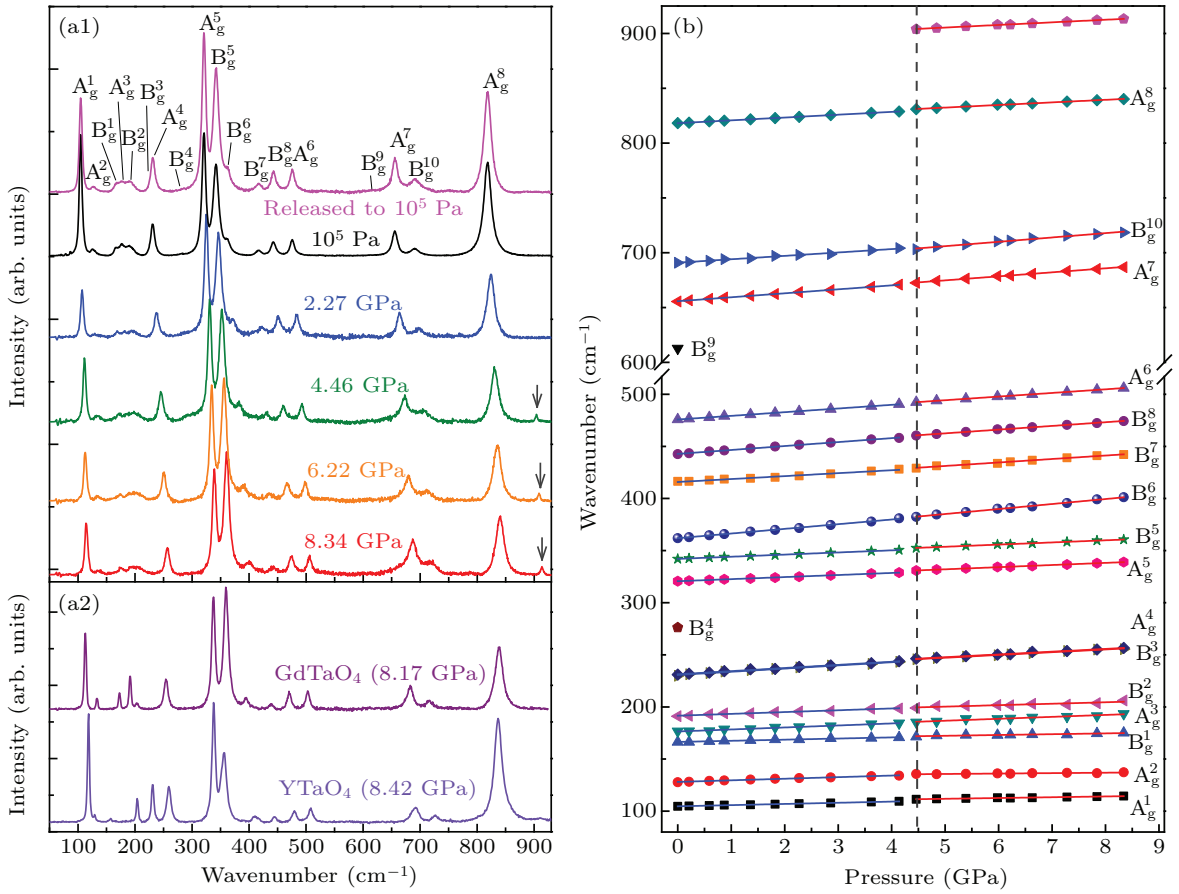


Fig. 5. (a1) Raman spectra of $GdYTaO_4$ at room temperature and various pressures. Raman modes are labeled according to Ref. [21]. Gray arrow indicates a peak appearing at the higher pressures. (a2) Raman spectra of $GdTaO_4$ and $YTaO_4$ at room temperature and pressures higher than 8 GPa. (b) Frequencies of Raman modes of $GdYTaO_4$ *versus* pressure. Blue and red solid lines represent linear fitting curves for the data in the lower (10^5 Pa–4.14 GPa) and higher (4.46 GPa–8.34 GPa) pressure ranges, respectively. Black dashed line indicates 4.46-GPa pressure.

Table 1. Frequencies at ambient pressure ω_0, pressure coefficients $\mathrm{d}\omega/\mathrm{d}P$, and pressure coefficient differences $\Delta(\mathrm{d}\omega/\mathrm{d}P)$ between lower (10^5 Pa–4.14 GPa) and higher (4.46 GPa–8.34 GPa) pressure ranges for Raman modes of $GdYTaO_4$.

Raman modes	ω_0 (cm^{-1})	$\mathrm{d}\omega/\mathrm{d}P$ (cm^{-1}/GPa)		$\Delta(\mathrm{d}\omega/\mathrm{d}P)$
		10^5 Pa – 4.14 GPa	4.46 GPa– 8.34 GPa	(cm^{-1}/GPa)
A_g^1	109.1	1.13	0.75	0.38
A_g^2	132.2	1.52	0.41	1.11
B_g^1	170.8	1.09	0.77	0.32
A_g^3	181.2	1.93	1.86	0.07
B_g^2	195.5	1.74	1.39	0.35
B_g^3	229.8	3.05	2.64	0.41
A_g^4	235.5	3.00	2.66	0.34
B_g^4	275.5	–	–	–
A_g^5	325.2	1.98	2.06	–0.08
B_g^5	346.5	2.05	2.07	-0.02
B_g^6	366.4	4.48	4.8	–0.32
B_g^7	420.9	2.82	3.34	–0.52
B_g^8	447.1	3.79	3.56	0.23
A_g^6	480.2	3.53	3.49	0.04
B_g^9	617.2	–	–	–
A_g^7	660.0	3.62	3.66	–0.04
B_g^{10}	695.4	3.1	3.96	–0.86
A_g^8	822.7	2.57	2.36	0.21
The mode appears at high pressures	–	–	2.37	–

As the Raman spectra in Fig. 5(a1) show, all the Raman modes of $GdYTaO_4$ shift toward higher frequencies with pressure increasing, indicating that the force constants between atoms involved in these modes are becoming stronger, because the force constant is proportional to the second power of phonon frequency.[24] This phenomenon can be explained by the enhancement of interaction among atoms due to the pressure-induced lattice shrinking.[24–26] It should be noted that a new peak appears at ~ 904 cm^{-1} under 4.46 GPa, and becomes stronger with pressure increasing. However, no extra peak is found in Raman spectra of $GdTaO_4$ and $YTaO_4$ in a pressure range larger than 8 GPa (see Fig. 5(a2)). This indicates that a phase transition for $GdYTaO_4$ might occur at 4.46 GPa. Evolutions of frequencies of the Raman modes (except B_g^4 and B_g^9, which are too weak to be traced) for $GdYTaO_4$ with pressure are analyzed. Slight discontinuities can be found in these evolutions at 4.46 GPa (see Fig. 5(b)), resulting in differences between the pressure coefficients of 10^5 Pa–4.14 GPa and those of 4.46 GPa–8.34 GPa for the Raman modes (see Table 1). This phenomenon coincides with the new Raman peak appearing and the discontinuity in the I_1/I_2 evolution, which could be another evidence for the phase transition deduction. In the process of decompression down to the ambient pressure, the Raman spectrum of $GdYTaO_4$ returns to the initial pattern (see Fig. 5(a1)), indicating that the pressure-induced phase transition is reversible for the pressure range attained in this research.

The stability of M-type structure under high pressure was discussed in Refs. [25–27]. The experimental results indicate M-type $GdNbO_4$ and $EuNbO_4$ can remain stable up to 25 GPa[25] and 20 GPa,[26] respectively. The large pressure stability of M-type rare-earth orthoniobates was explained by the flexibility of LnO_8 (Ln = Gd, Eu) polyhedra[25,26] which can accommodate the increasing repulsive and steric stresses induced by pressure, thereby avoiding the transformation to a high pressure phase.[25] This is useful for understanding why the Raman modes observed at ambient pressure for M-type $GdYTaO_4$ can keep well at high pressures. However, the difference between compressibilities of GdO_8 and YO_8 polyhedron can complicate the structural evolution of $GdYTaO_4$ under pressure. The research of Ref. [27] indicates M-type $GdNbO_4$ doped with Eu^{3+} undergoes a phase transition to M′-type structure (with a space group symmetry of $P2/a$) at 6.2 GPa, which can be an example for exhibiting the influence of dopants on the pressure stability of M-type structure. As one of the main fingerprints for ascertaining phase transition, the new Raman peaks of Eu^{3+}:$GdNbO_4$ found at high pressures are in a spectral range less than 300 cm^{-1},[27] which is much lower than the new Raman peak of $GdYTaO_4$ observed at high pressures. Therefore, the structure of $GdYTaO_4$ under pressures beyond 4.46 GPa should not be of M′-type, indicating the structural symmetry of $GdYTaO_4$ might not be changed much. The research of Ref. [28] reveals that a subtle phase transition could be triggered at a relatively low pressure for a solid solution (like the sample studied) which seems constituted by two materials with similar structures. This can also support the phase transition deduction for $GdYTaO_4$ under high pressure. Moreover, according to the research of

Ref. [29] and the observed small difference between the Raman spectra of $GdYTaO_4$ measured under pressures below and above 4.46 GPa, the phase transition can be deduced to be isostructural further.

4. Conclusions

The temperature- and pressure-dependent luminescence from $^3H_4 \rightarrow {}^3H_6$ transition of Tm^{3+}:$GdYTaO_4$ are studied for the first time. Two main emission peaks at around 790 nm and 793 nm are observed. Their intensity ratio I_1/I_2 evolves exponentially with temperature, showing a potential application in temperature sensing. The highest sensitivity of I_1/I_2 is found at 32 K to be a value of 0.014 K^{-1}. The energy difference between the two emission peaks increases linearly with pressure rising in a rate of 0.38 meV/GPa, which will be useful for pressure sensing in NIR spectral range. The emission lifetimes of the two emission peaks decrease with pressure rising, which is due to the probability increasing of the CR process. The I_1/I_2 evolution with pressure is also investigated, and a non-monotonic behavior is revealed. The structural stability of M-type $GdYTaO_4$ under high pressures is discussed based on Raman measurements. The recorded Raman spectra indicate that an isostructural phase transition can occur at $\sim$ 4.46 GPa.

Acknowledgements

Project supported by the National Natural Science Foundation of China (Grant No. 11804047) and the Science and Technology Development Program of Jilin City, China (Grant No. 201831733).

References

[1] Sun J S, Li X P, Wu J L, Li S W, Shi L L, Xu S, Zhang J S, Cheng L H and Chen B J 2017 *Acta Phys. Sin.* **66** 100201 (in Chinese)
[2] Dai L, Liu C R, Han X B, Wang L P, Shao Y and Xu Y H 2018 *Chin. Phys. B* **27** 114217
[3] Nyk M, Kumar R, Ohulchanskyy T Y, Bergey E J and Prasad P N 2008 *Nano Lett.* **8** 3834
[4] Zheng W, Zhu H M, Li R F, Tu D T, Liu Y S, Luo W Q and Chen X Y 2012 *Phys. Chem. Chem. Phys.* **14** 6974
[5] Li J, Zhang J H, Zhang X, Hao Z D and Luo Y S 2014 *J. Alloys Compd.* **583** 96
[6] Zhang X Y, Wang J G, Xu C L, Pan Y, Hou Z Y, Ding J, Cheng L and Gao D L 2016 *Acta Phys. Sin.* **65** 204205 (in Chinese)
[7] Quintanilla M, Cantelar E, Cussó F, Barreda-Argüeso J A, González J, Valiente R and Rodríguez F 2015 *Opt. Mater. Express* **5** 1168
[8] Ren X K, Du C L, Li C B, Yu L, Zhao J Q and Ruan S C 2016 *Chin. Phys. Lett.* **33** 114203
[9] Dou R Q, Zhang Q L, Gao J Y, Chen Y Z, Ding S J, Peng F, Liu W P and Sun D L 2018 *Crystals* **8** 55
[10] Dou R Q, Zhang Q L, Liu W P, Luo J Q, Wang X F, Ding S J and Sun D L 2015 *Opt. Mater.* **48** 80
[11] Nakauchi D, Koshimizu M, Okada G and Yanagida T 2017 *Radiat. Meas.* **106** 129
[12] Peng F, Yang H J, Zhang Q L, Luo J Q, Sun D L, Liu W P, Sun G H, Dou R Q, Wang X F and Xing X 2015 *Opt. Mater. Express* **5** 2536
[13] Yang H J, Peng F, Zhang Q L, Guo C X, Shi C S, Liu W P, Sun G H, Zhao Y P, Zhang D M, Sun D L, Yin S T, Gu M and Mao R H 2014 *Cryst. Eng. Comm.* **16** 2480
[14] Wu P, Zhou Y X, Wu F S, Hu M Y, Chong X Y and Feng J 2019 *J. Am. Ceram. Soc.* **102** 7656
[15] Klotz S, Chervin J C, Munsch P and Le March G 2009 *J. Phys. D: Appl. Phys.* **42** 075413
[16] Mao H K, Xu J and Bell P M 1986 *J. Geophys. Res.* **91** 4673
[17] Li D Y, Wang Y X, Zhang X R, Yang K, Liu L and Song Y L 2012 *Opt. Commun.* **285** 1925
[18] Tiseanu C, Lupei A and Lupei V 1995 *J. Phys.: Condens. Matter* **7** 8477
[19] Wamsley P R and Bray K L 1994 *J. Lumin.* **60–61** 188
[20] Barnett J D, Block S and Piermarini G J 1973 *Rev. Sci. Instrum.* **44** 1
[21] Siqueira K P F and Carvalho G B 2011 *Dalton Trans.* **40** 9454
[22] Feng J, Shian S, Xiao B and Clarke D R 2014 *Phys. Rev. B* **90** 094102
[23] Blasse G 1973 *J. Solid State Chem.* **7** 169
[24] Long Y W, Yang L X, Yu Y, Li F Y, Yu R C, Ding S, Liu Y L and Jin C Q 2006 *Phys. Rev. B* **74** 054110
[25] Pellicer-Porres J, Garg A B, Vázquez-Socorro D, Martínez-García D, Popescu C and Errandonea D 2017 *J. Solid State Chem.* **251** 14
[26] Garg A B, Rao R, Errandonea D, Pellicer-Porres J, Martinez-Garcia D and Popescu C 2020 *J. Appl. Phys.* **127** 175905
[27] Hou J W, Zhou R, Zhang J W, Wang Z P, Zhang Z M and Ding Z J 2017 *J. Phys. Chem. C* **121** 14787
[28] Bandiello E, Errandonea D, Piccinelli F, Bettinelli M, Díaz-Anichtchenko D and Popescu C 2019 *J. Phys. Chem. C* **123** 30732
[29] Gonzalez-Platas J, Rodriguez-Hernandez P, Muñoz A, Rodríguez-Mendoza U R, Nénert G and Errandonea D 2019 *Crystals* **9** 643